


# A novel six-dimensional disturbance force and moment simulator for simulation of space micro-vibration environment

Journal of Vibration and Control  
2022, Vol. 0(0) 1–12  
© The Author(s) 2022  
Article reuse guidelines:  
[sagepub.com/journals-permissions](https://sagepub.com/journals-permissions)  
DOI: 10.1177/10775463221101943  
[journals.sagepub.com/home/jvc](https://journals.sagepub.com/home/jvc)  
SAGE

Xiaoming Wang<sup>1,2,#</sup>, Shuai He<sup>1,2,#</sup>, Zhenbang Xu<sup>1,2</sup> , Hang Li<sup>1,2</sup>,  
Huayang Sai<sup>1,2,3</sup>, Jianfeng Yang<sup>4</sup>, and Lin Li<sup>5,6</sup>

## Abstract

A novel six-dimensional disturbance force and moment simulator was developed because of the lack of a suitable vibration source for use in ground experiments. First, the dynamic relationship between the disturbance force, the disturbance moment generated at the center of the simulator platform, and the excitation forces of the six uniaxial actuators was established using the equivalent principle of force system. Then, the simulator structure was introduced and a modal analysis of this structure was performed. Finally, the simulator system was tested experimentally in both single-frequency experiments and multi-frequency experiments. The results obtained showed that the maximum error between the experimental values and the target values was 2.96%, which verified the correctness of the theoretical model of the six-dimensional disturbance force and moment simulator. Additionally, the multi-dimensional micro-vibration generation performance of the new simulator was verified. The proposed six-dimensional disturbance force and moment simulator can provide a micro-vibration environment to replace the real disturbance sources used in ground experiments and solve the problems caused by the lack of a vibration source for use in ground-based experiments.

## Keywords

micro-vibration, simulator, disturbance force, disturbance moment, equivalent principle of force system

## 1. Introduction

As a result of the continuous development of space-based optical load technology, higher imaging equipment resolutions are increasingly required. The space micro-vibration environment can affect the pointing accuracy and attitude stability of a space-based optical load seriously, reducing its resolution and thus also affecting the imaging quality obtained (Lin et al., 2018; Sun et al., 2018). Several researchers have used physical methods to make their systems vibration-resistant or to ensure that objects do not vibrate (Bianco et al., 2017; Hehlen et al., 2018). However, because of the complexity of the space environment, these methods were unsuitable for use with space-based optical loads. Because the main source of space micro-vibration is flight reaction wheel (Luo et al., 2013; Sun et al., 2018), some researchers isolated the vibration of reaction flywheel itself (Zhou et al., 2011), others designed vibration isolation devices (Chen et al., 2020; Liu et al., 2015; Qin et al., 2020; Xu et al., 2019b; Zhang et al., 2016). These vibration isolation devices are widely used because of their good stability. To assess the performance of these isolation devices, the imaging effects on space-based optical loads must

<sup>1</sup>CAS Key Laboratory of On-orbit Manufacturing and Integration for Space Optics Systems, Changchun Institute of Optics, Fine Mechanics and Physics, Chinese Academy of Sciences, Changchun, China

<sup>2</sup>Innovation Laboratory of Space Robot Systems, Space Robotics Engineering Center, Changchun Institute of Optics, Fine Mechanics and Physics, Chinese Academy of Sciences, Changchun, China

<sup>3</sup>University of Chinese Academy of Sciences, Beijing, China

<sup>4</sup>China Electronic Product Reliability and Environmental Testing Research Institute, Guangzhou, China

<sup>5</sup>Space Optoelectronic Measurement and Perception Lab., Beijing Institute of Control Engineering, Beijing, China

<sup>6</sup>China Academy of Space Technology, Beijing, China

Received: 24 January 2022; revised: 7 April 2022; accepted: 29 April 2022

<sup>#</sup>Xiaoming Wang and Shuai He contributed equally to this work.

## Corresponding authors:

Zhenbang Xu, CAS Key Laboratory of On-orbit Manufacturing and Integration for Space Optics Systems, Changchun Institute of Optics, Fine Mechanics and Physics, Chinese Academy of Sciences, Changchun, Jilin 130033, China.

Email: [xuzhenbang@ciomp.ac.cn](mailto:xuzhenbang@ciomp.ac.cn)

Lin Li, Space Optoelectronic Measurement and Perception Lab., Beijing Institute of Control Engineering, Beijing 100190, China.

Email: [cast\\_lilin@163.com](mailto:cast_lilin@163.com)

be tested experimentally in micro-vibration environments. The provision of a suitable vibration source for ground experiments is urgently required.

At present, the most commonly used method is to perform the optical load imaging experiment under the condition where the whole machine is in the micro-vibration environment. Because the entire machine is tested, two methods can be used to simulate the micro-vibration environment: the first is to use real disturbance equipment such as a flight reaction wheel, and the second is to use a simulator.

Liu et al. (2007) used a flight reaction wheel to generate the required disturbance and connected it to a structural verification unit to measure the degree of disturbance produced by the flight reaction wheel. However, disturbance generation using the flight reaction wheel increases the experimental costs greatly and requires a high level of research funding. In addition, the disturbance that can be provided by real disturbance equipment often has a comparatively fixed profile, which makes it impossible to assess the optical load performance variation effectively at different vibration levels, and this will affect subsequent studies.

To solve this problem, some research institutions have used simulators as disturbance sources to develop the multi-dimensional electromagnetic excitation equipment required. Park et al. from South Korea studied two generations of multi-dimensional micro-vibration simulators. The first-generation disturbance force simulator (Park and Han, 2012) simply elaborated on the idea that multi-dimensional disturbances could be simulated using six identical single-axis actuators but did not produce a simulator as a physical object. The second-generation disturbance force simulator (Han et al., 2014) could produce the disturbance force required in three perpendicular directions, but could not meet the ground-based testing requirements in terms of the degrees of freedom available. A six-dimensional micro-vibration simulator based on the Gough–Stewart configuration was fabricated in the Robotics Center of the CAS Changchun Institute of Optics, Fine Mechanics and Physics (Wang et al., 2018; Xu et al., 2019a; Yang et al., 2016) that realized the vibration output of a multi-frequency line spectrum. Although this simulator met the requirements for degrees of freedom, the complexity of the dynamic model used could affect the device's control accuracy.

With this background, this paper presents a novel six-dimensional disturbance force and moment simulator that offers good decoupling properties and simple control. When compared with the Stewart configuration, the structure of the proposed configuration is both simple and decoupled. There is no need for hinges or other moving mechanisms and the effects of nonlinear factors such as the clearance friction are avoided, which means that the linearity of the structure is good and the control precision is high. A theoretical model of the disturbance force and moment

simulator is established using the principle of force system equivalence in this paper. When compared with modeling methods for multi-body systems, that is, the Newton–Euler method and methods based on the Lagrange equation and the Kane equation (Asadi and Sadati, 2017; Oftadeh, 2010; Wu et al., 2015), the model based on the principle of force system equivalence is easier to understand. The correctness of the proposed theoretical model was verified by the results of experiments.

The remainder of the paper is organized as follows. In Section 2, the theoretical models of the uniaxial actuator and the complete simulator machine are established. Additionally, the dynamic relationships between the disturbance force, the moment generated at the center of simulator platform and the excitation forces of the six uniaxial actuators are obtained. The working principle of the simulator is also introduced. Section 3 then introduces the structure of the six-dimensional disturbance force and moment simulator and analyzes the natural frequency of the simulator using the finite element method. Section 4 verifies the correctness of the theoretical model via experimental testing, single-frequency tests and multi-frequency tests are applied to the simulator. Finally, Section 5 draws conclusions about the performance of the proposed six-dimensional disturbance force and moment simulator.

## 2. Theoretical modeling

The six-dimensional disturbance force and moment simulator designed in this paper is composed of six single-axis actuators. Each single-axis actuator can provide a disturbance force in one direction and the spatial positions of the six single-axis actuators can be arranged appropriately to realize simulations of the disturbance force and moment in six directions. In this section, a theoretical model of the disturbance force for a single uniaxial actuator is established. Furthermore, the working principle that allows the six-dimensional disturbance force and moment simulator to provide the six-degrees-of-freedom disturbance and moment is introduced. Then, a dynamic model of the entire machine is established according to the principle of force system equivalence.

### 2.1. Theoretical modeling of uniaxial actuator

A theoretical model of a single uniaxial actuator is established in this section to determine the relationship between the reaction force  $f$  at the mounting surface of the actuator and the excitation force  $f_d$  of the uniaxial actuator. This uniaxial actuator is equivalent to a single-degree-of-freedom system. A schematic diagram of the uniaxial actuator is shown in Figure 1. In the diagram,  $f$  represents the reaction force of the actuator acting on the mounting surface,  $k$  is the stiffness of the electromagnetic actuator,  $c$  is the damping of the electromagnetic actuator,  $m$  is the

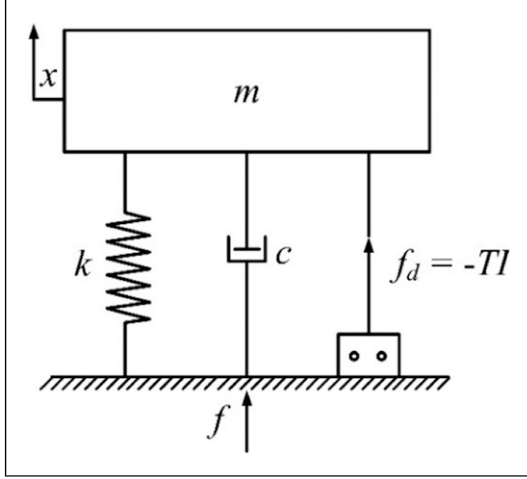


**Figure 1.** Schematic diagram of the uniaxial actuator.

moving mass of the electromagnetic actuator,  $f_d$  is the excitation force of the electromagnetic actuator and is proportional to the electromagnetic actuator current  $I$ , and the proportional coefficient is  $T$ .  $x$  represents the displacement of the single-axis actuator,  $\dot{x}$  represents the speed of the single-axis actuator, and  $\ddot{x}$  represents the acceleration of the single-axis actuator.

Performing a force analysis of a single-degree-of-freedom system enables the following equation to be obtained

$$m\ddot{x} + c\dot{x} + kx = f_d \quad (1)$$

After a Laplace transformation, the equation above can be shown as follows

$$X(s) = \frac{F_d(s)}{mS^2 + cS + k} \quad (2)$$

The reaction force at the mounting surface can then be expressed as

$$F(S) = \frac{-mS^2 F_d(S)}{mS^2 + cS + k} \quad (3)$$

For  $S = j\omega$ ,  $\lambda = \frac{\omega}{\omega_p}$  is the frequency ratio.  $\beta$  is the amplitude ratio of disturbing force (spring vibration to base) to excitation force of voice coil motor,  $\phi$  is the phase ratio of disturbing force to exciting force, and then

$$\begin{aligned} \beta &= \left| \frac{F(j\omega)}{F_d(j\omega)} \right| = \left| \frac{\omega^2}{-\omega^2 + 2\xi_p \omega_p \omega j + \omega_p^2} \right| \\ &= \frac{1}{\sqrt{\left(\frac{1}{\lambda^2} - 1\right)^2 + \frac{4\xi_p^2}{\lambda^2}}} \end{aligned} \quad (4)$$

$$\phi = \arctan \frac{2\xi_p \lambda}{1 - \lambda^2} \quad (5)$$

$\omega_p$  is the natural frequency of the electromagnetic actuator,  $\xi_p$  is the damping ratio of the electromagnetic actuator, and the two parameters can be expressed as

$$\omega_p = \sqrt{\frac{k}{m}}, \xi_p = \frac{c}{2m\omega_p} \quad (6)$$

The stiffness  $k$  is 3.472 N/mm and the moving mass  $m$  is 0.516 kg. The damping ratio  $\xi_p$  is 0.05 (This value is an empirical value, and the damping of the actual system needs to be corrected by the experimental data). Equations (4) and (5) can be used to obtain the amplitude-frequency response curve and the phase-frequency response curve of the disturbance force and the excitation force, as shown in Figure 2. Because the excitation frequency is higher than the natural frequency, the amplitude ratio decreases with increasing frequency and gradually converges to a value of 1. In addition, with increasing frequency, the phase converges to a value of  $180^\circ$  away from the natural frequency.

## 2.2. Theoretical modeling of six-dimensional disturbance force and moment simulator

The six-dimensional disturbance force and moment simulator realizes the required six-dimensional force and moment output through the cooperative operation of six single-axis actuators arranged spatially. Figure 3 shows the installation positions of the actuators and the complete coordinate system for the simulator. The axis of uniaxial actuator 5 coincides with the  $x$  axis and the distance from the origin to this actuator is  $r_1$ . The actuator 5 can produce disturbing force in  $x$  direction when working. The axis direction of uniaxial actuator 4 coincides with the  $y$  axis and the distance from this actuator to the origin is  $r_1$ . The actuator 4 can produce disturbing force in  $y$  direction when working. The axes of actuators 1, 2, and 3 are all parallel to the  $z$  axis and are uniformly distributed around the  $z$  axis at angles of  $120^\circ$  relative to each other. In addition, the distance from the origin to each of these actuators is  $r_2$ . The distribution of the actuators is shown in Figure 3 and this configuration can produce the  $z$  axis disturbance force and the disturbance moment around both the  $x$  axis and the  $y$  axis. The angle between the axis of actuator 6 and the negative direction of the  $x$  axis is  $30^\circ$ . In addition, the distance from this actuator to the origin is  $r_3$  and this actuator can produce the disturbance moment around the  $z$  axis and the disturbance force along both the  $x$  axis and the  $y$  axis.

The vectors that point from the origin toward the center of each installation position are called the vector diameters, which are recorded as

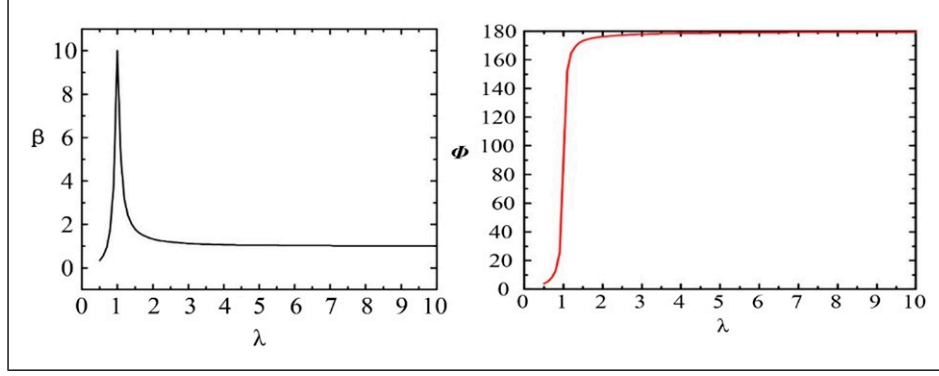


**Figure 2.** Amplitude-frequency and Phase-frequency response curve.

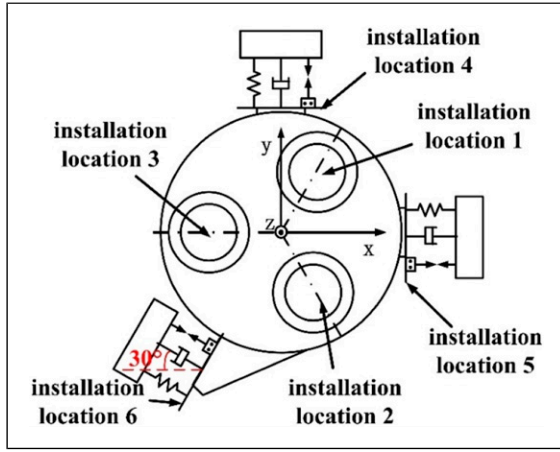


**Figure 3.** Distribution of the actuators in the simulator.

$$r_i = [x_i \ y_i \ z_i]^T (i = 1, 2, \&z, 6) \quad (7)$$

where  $f_1, f_2, f_3, f_4, f_5$ , and  $f_6$  represent the disturbance forces generated by the six uniaxial actuators at their respective contact surfaces. The installation radius for each of actuators 1–3 is  $r_1$ ; the distance from both actuators 4 and 5 to the origin is  $r_2$ , and the distance from actuator 6 to the origin is  $r_3$ . The disturbance vectors for the actuators can then be shown as follows

$$\begin{aligned} F_i &= [0 \ 0 \ f_i]^T (i = 1, 2, 3) \\ F_4 &= [0 \ f_4 \ 0]^T \\ F_5 &= [f_5 \ 0 \ 0]^T \\ F_6 &= \left[ -\frac{\sqrt{3}}{2}f_6 \ \frac{1}{2}f_6 \ 0 \right]^T \end{aligned} \quad (8)$$

Based on the equivalent principle of force system, the forces generated by the six uniaxial actuators are equivalent to the force and moment generated at the center of the origin. The equivalent equations for this condition are shown as follows

$$\begin{aligned} f_{0i} &= F_i \\ m_{0i} &= r_i \times F_i \end{aligned}$$

According to the equations above, the six-dimensional disturbance force and moment generated at the center of the six-dimensional disturbance force and moment simulator platform can then be obtained as follows

$$\begin{aligned} f_0 &= \begin{bmatrix} f_x \\ f_y \\ f_z \\ m_x \\ m_y \\ m_z \end{bmatrix} \\ &= \begin{bmatrix} 0 & 0 & 0 & 0 & 1 & -\sqrt{3}/2 \\ 0 & 0 & 0 & 1 & 0 & -1/2 \\ 1 & 1 & 1 & 0 & 0 & 0 \\ \sqrt{3}r_1/2 & -\sqrt{3}r_1/2 & 0 & 0 & 0 & 0 \\ -r_1/2 & -r_1/2 & r_1 & 0 & 0 & 0 \\ 0 & 0 & 0 & 0 & 0 & -r_3 \end{bmatrix} \begin{bmatrix} f_1 \\ f_2 \\ f_3 \\ f_4 \\ f_5 \\ f_6 \end{bmatrix} \end{aligned} \quad (10)$$

It is assumed that the natural frequency and damping characteristics are the same for each actuator in the disturbance platform. In addition, equation (4) can be brought into equation (10) and the relationship between the disturbance force  $F_0$  of the platform and the electromagnetic excitation force  $F_d$  in the frequency domain can then be obtained as follows

$$|F_0| = \frac{1}{\sqrt{\left(\frac{1}{\lambda^2} - 1\right)^2 + \frac{4\lambda^2}{\lambda^2}}}$$

$$\begin{bmatrix} 0 & 0 & 0 & 0 & 1 & -\sqrt{3}/2 \\ 0 & 0 & 0 & 1 & 0 & -1/2 \\ 1 & 1 & 1 & 0 & 0 & 0 \\ \sqrt{3}r_1/2 & -\sqrt{3}r_1/2 & 0 & 0 & 0 & 0 \\ -r_1/2 & -r_1/2 & r_1 & 0 & 0 & 0 \\ 0 & 0 & 0 & 0 & 0 & -r_3 \end{bmatrix} \begin{bmatrix} F_{1d} \\ F_{2d} \\ F_{3d} \\ F_{4d} \\ F_{5d} \\ F_{6d} \end{bmatrix} \quad (11)$$

### 3. Structure of six-dimensional disturbance force and moment simulator

The proposed six-dimensional disturbance force and moment simulator consists of an installation platform and six identical uniaxial actuators, as shown in Figure 4. When the uniaxial actuator 5 works, it can generate the disturbing force in the  $x$  direction. When the uniaxial actuator 4 works, it can generate the disturbing force in the  $y$  direction. When the actuators 1, 2 and 3 work, it can generate the disturbing force in the  $z$  direction and the disturbing torque around the

$x$  and  $y$  axes. When the actuator 6 works, it can generate the disturbing torque around the  $z$  axis and the disturbing force in the  $x$  and  $y$  directions. The working principle diagram of the proposed simulator is shown in Figure 5. The six-dimensional disturbance simulator is a kind of vibration source equipment, which can replace the real disturbance source to provide micro-vibration environment in ground experiment. The simulator is installed on the experimental load, and the optical load and the simulator are suspended by the suspension system to unload the gravity. The six actuators can produce the six-dimensional disturbance force and moment characteristics required to realize simulations of the multi-dimensional micro-vibrations that occur in space.

#### 3.1. Structural design of single-axis actuator

The detailed structure of the uniaxial actuator is shown in Figure 6 and illustrates that the main body of the actuator is largely composed of a voice coil motor, a motor shaft, and a sleeve. The stator of the voice coil motor is installed at the bottom of the sleeve, and the sleeve functions as both a supporting structure and a protective structure for the motor. The motor mover is connected to the motor shaft to drive the upper and lower springs into their axial motions. The actuator uses a double-layer spring plate structure with low axial stiffness and high radial stiffness characteristics that can ensure the actuator will move along the axial direction. The motor mover, motor shaft and end cover structures provide the actual mass for the uniaxial actuator.

As the power source of the simulator, voice coil motor provides axial driving force for the actuator and drives the upper and lower spring plates to move axially. As an important part of the actuator, the spring can unload the gravity and ensure the actuator to move along the axial direction.

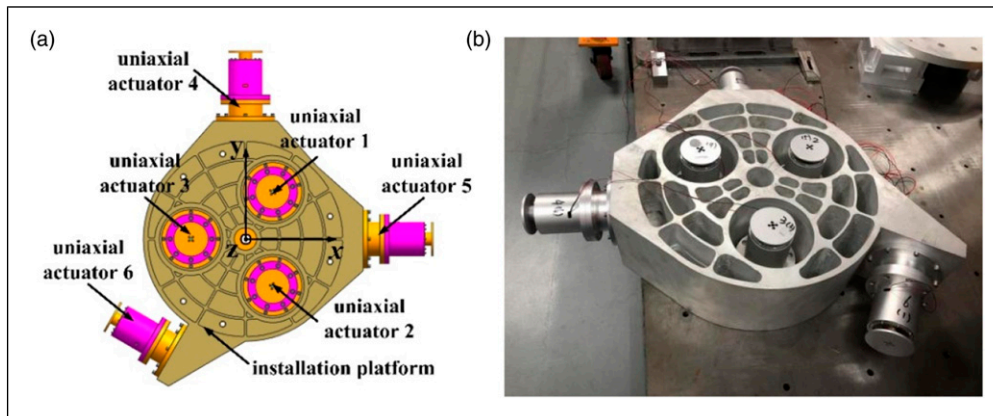


**Figure 4.** Structure of the six-dimensional disturbance force and moment simulator. (a) Three-dimensional structure. (b) Physical device.



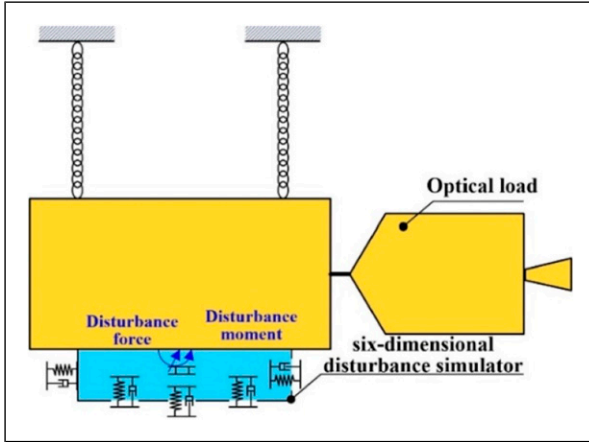


**Figure 5.** Working principle diagram of the proposed simulator.

The actuator of the simulator adopts double-layer spring plate structure, which can better ensure the axial movement of the actuator. The axial stiffness of the double-layer spring plate directly affects the motion ability of the driving leg, and the thickness, pattern, material, and processing technology of the spring plate will affect its characteristics. Considering that the spring plate should have low axial stiffness and small maximum stress, we adopt multi-layer surrounding pattern (Wang, 2017), as shown in Figure 6. Using the finite element analysis method, the maximum stress of the spring plate is 193 MPa and the axial stiffness of the spring plate is 1.736 N/mm. The uniaxial actuator is a double spring plate configuration, so the stiffness of the uniaxial actuator is twice that of a leaf spring.

### 3.2. Fundamental frequency analysis

The modal analysis of the platform is carried out by using the finite element method. The solid element is used to model the installation platform and actuators, multi point constraint simulation screw connection is adopted between

the installation platform and actuators. The finite element model of the whole simulator is shown in Figure 7(a). When the “zero displacement” constraint is applied to the base of the installation platform, the first seven fundamental frequencies of the whole simulator are obtained. Among them, the first six modes are 13.415 Hz, and the vibration mode is the axial vibration of the actuator. The seventh-order fundamental frequency is 265 Hz and the vibration mode is the bending vibration of the actuator. The vibration modes from the first-order fundamental frequency to the seventh-order fundamental frequency are shown in Figure 7(b)–(h).

## 4. Experimental testing of six-dimensional disturbance force and moment simulator

In order to verify the correctness of the theoretical model established in Section 2.2 and the multi-dimensional micro-vibration generation performance of the simulator, experimental testing system is carried out in this section. Structural parameters of simulator are listed in Table 1. Because the measurement error of the structural parameters of the simulator will affect the simulation accuracy of the simulation platform, a feedback iterative control algorithm based on the theoretical model is proposed.

### 4.1. Iterative control algorithm for simulation of disturbance force and moment

There is an error between the actual structural parameters of the simulator and the measured values of the simulator, which will cause the actual disturbance force output by the simulator to be inconsistent with the target value. In order to improve the accuracy of micro-vibration environment simulation, a comparison column iterative control algorithm is proposed based on the theoretical model of the simulator. The control law is designed as follows.

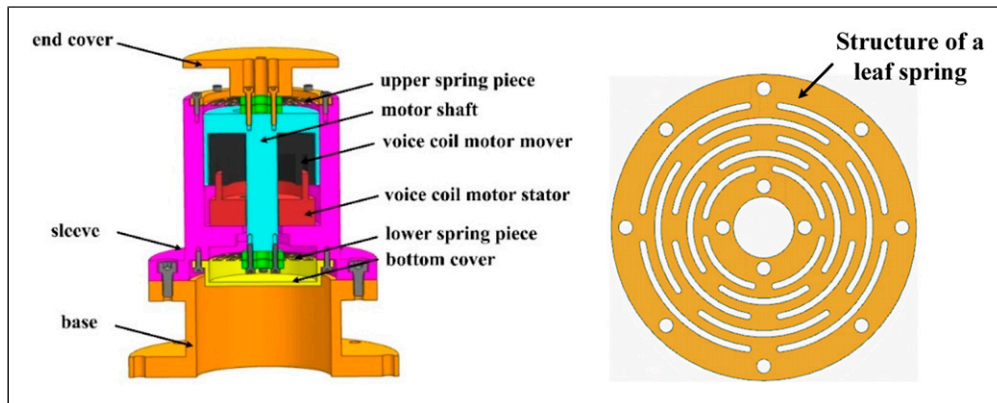


**Figure 6.** Detailed structural diagram of the uniaxial actuator.

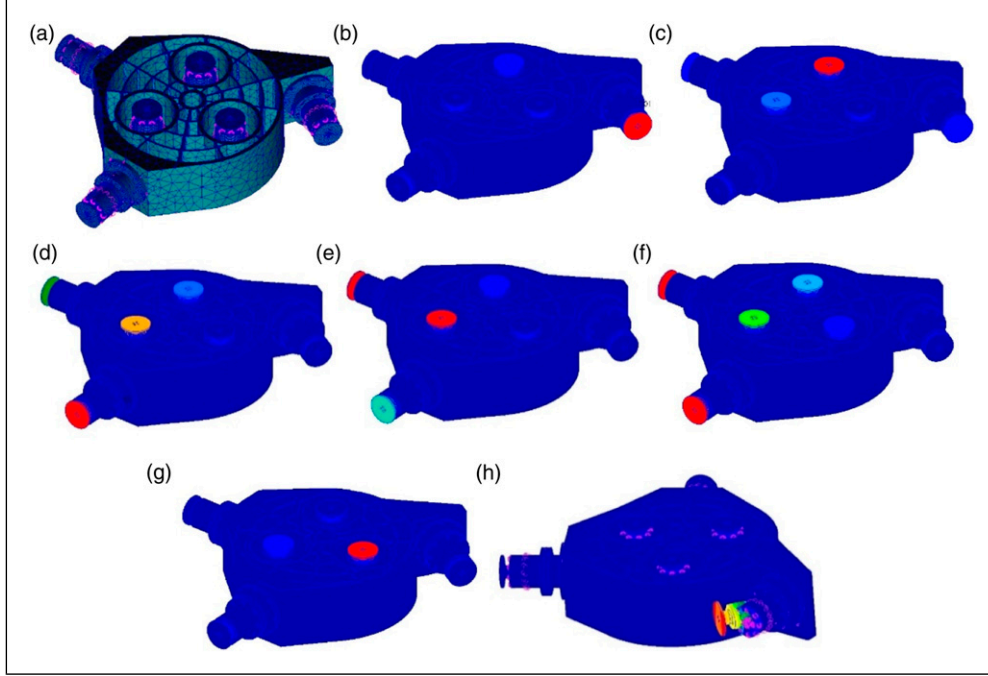


**Figure 7.** The vibration modes from the first-order fundamental frequency to the seventh-order fundamental frequency. (a) The finite element model (b) The first-order (c) The second-order, (d) The third-order (e) The fourth-order (f) The fifth-order (g) The sixth-order (h) The seventh-order.

**Table 1.** Structural parameters of the simulator.

Structural parameters	Parameters, m
Distance $x_1$ from actuator 1 to platform center in x direction	0.06
Distance $x_2$ from actuator 2 to platform center in x direction	0.06
Distance $x_3$ from actuator 3 to platform center in x direction	0.12
Distance $x_6$ from actuator 6 to platform center in x direction	0.294
Distance $y_1$ from actuator 1 to platform center in y direction	0.06
Distance $y_2$ from actuator 2 to platform center in y direction	0.06
Distance $y_3$ from actuator 3 to platform center in y direction	0.00

$Y_d(t)$  is the expected trajectory of the disturbance force and moment to be tracked using control system, where

$$Y_d = F_0^d \quad (12)$$

$Y_n(t)$  is the  $n^{\text{th}}$  output of the system, where

$$Y_n = F_0^n \quad (13)$$

Then, the control law of the system can be designed as follows

$$Y_{n+1} = K_n Y_d \quad (14)$$

where  $K_n$  is a  $6 \times 6$  iterative coefficient matrix that can be expressed as

$$K_n = \begin{pmatrix} k_1 & 0 & 0 & 0 & 0 & 0 \\ 0 & k_2 & 0 & 0 & 0 & 0 \\ 0 & 0 & k_3 & 0 & 0 & 0 \\ 0 & 0 & 0 & k_4 & 0 & 0 \\ 0 & 0 & 0 & 0 & k_5 & 0 \\ 0 & 0 & 0 & 0 & 0 & k_6 \end{pmatrix} \quad (15)$$

where  $n$  is the number of iterations. When  $n=0$ ,  $K_0=E_6$ ,  $E_6$  represents the identity matrix of  $6 \times 6$ . When  $n>0$ , the matrix can be expressed as

$$k_p = \frac{Y_{d,p}}{Y_{n,p}} \quad (16)$$

Figure 8 shows the iterative control flow chart for the six-dimensional disturbance force and moment simulator for

simulation of multi-dimensional disturbances. The first set of experimental values was obtained after inputting the target value, and the iterative coefficient matrix was then calculated based on the experimental value and the target value. The excitation force for each driving leg was

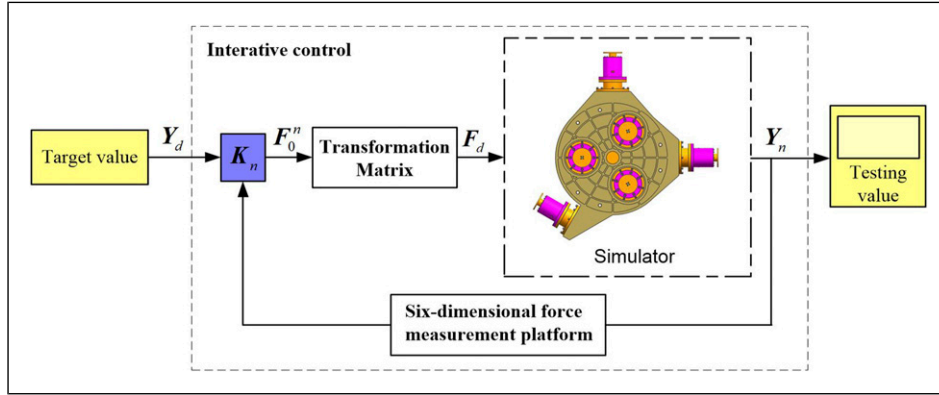


Figure 8. Iterative control flow chart for the simulator.

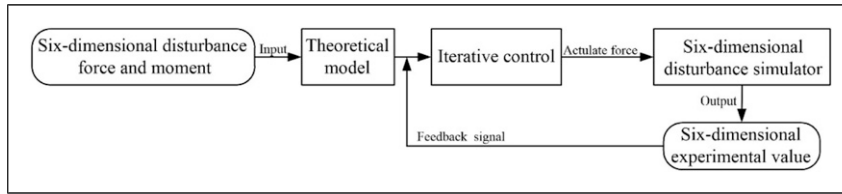


Figure 9. Disturbance force and moment planning scheme.

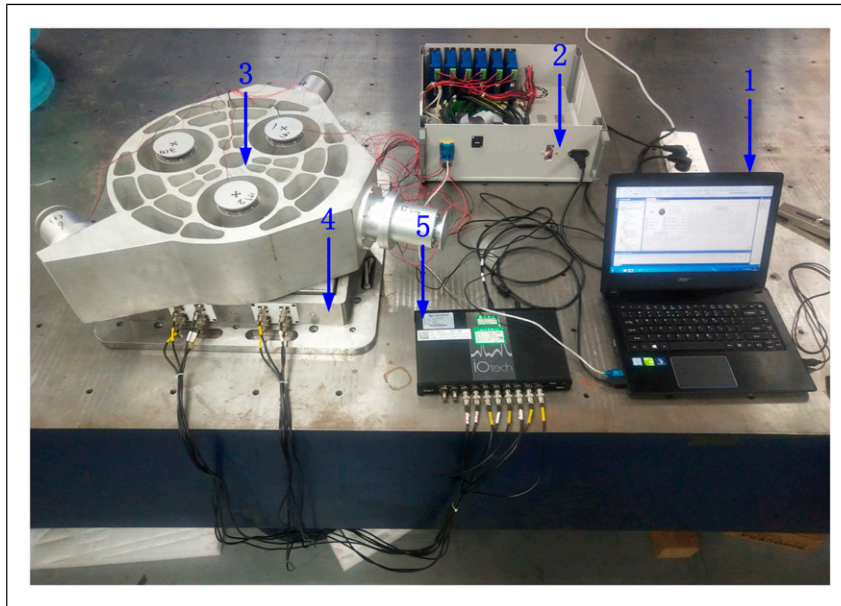


Figure 10. Test setup for the disturbance force and moment simulator.

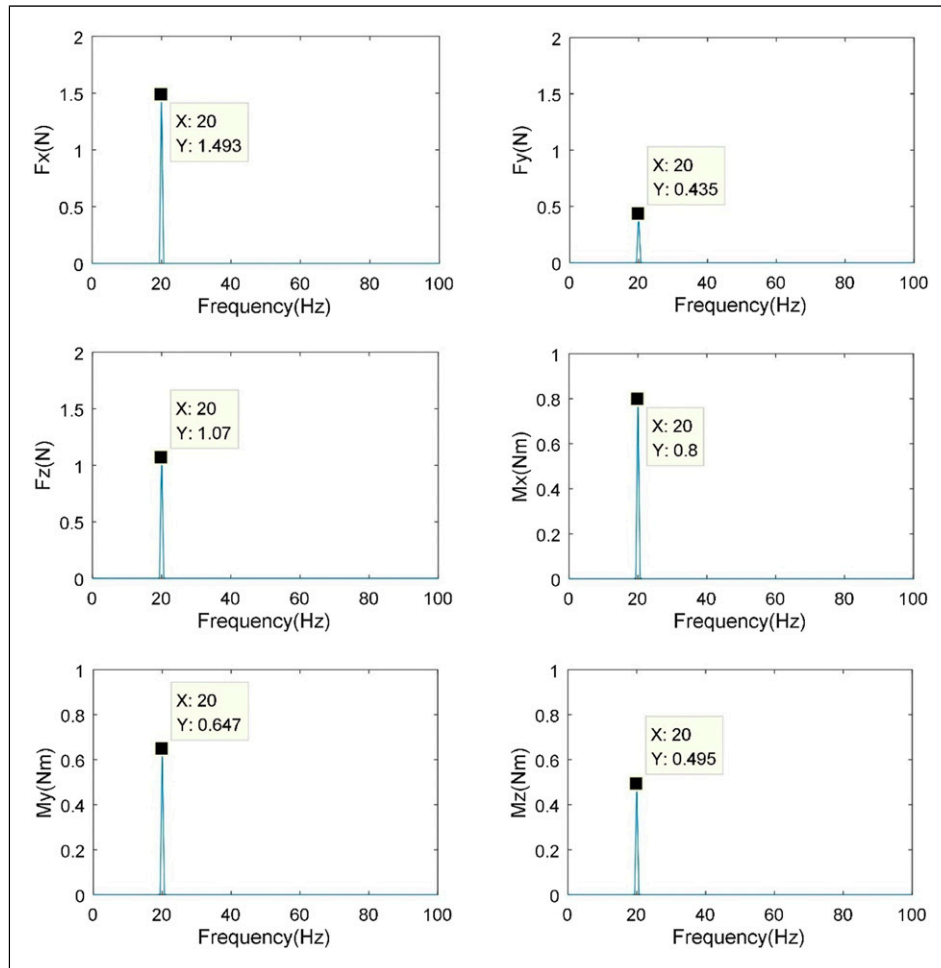


**Table 2.** Single-frequency disturbance force and moment target and experimental values.

Frequency (Hz)		F <sub>x</sub> (N)	F <sub>y</sub> (N)	F <sub>z</sub> (N)	M <sub>x</sub> (Nm)	M <sub>y</sub> (Nm)	M <sub>z</sub> (Nm)
20	Target value	1.50	0.43	1.05	0.80	0.65	0.50
	Testing value	1.493	0.435	1.07	0.8	0.647	0.495
	Relative error	0.47%	1.16%	1.90%	0%	0.46%	1.00%

**Table 3.** Multi-frequency disturbance force and moment target and experimental values.

Frequency (Hz)		F <sub>x</sub> (N)	F <sub>y</sub> (N)	F <sub>z</sub> (N)	M <sub>x</sub> (Nm)	M <sub>y</sub> (Nm)	M <sub>z</sub> (Nm)
30	Target value	1.43	0.46	1.4	0.84	0.65	1.44
	Testing value	1.432	0.451	1.416	0.841	0.642	1.4
	Relative error	0.14%	1.96%	1.14%	1.06%	1.23%	2.78%
60	Target value	1.43	0.65	1.45	1.35	1.2	1.44
	Testing value	1.428	0.64	1.42	1.39	1.207	1.403
	Relative error	0.14%	1.54%	2.07%	2.96%	0.58%	2.57%
90	Target value	1.5	0.86	1.44	1.5	1.35	1.4
	Testing value	1.49	0.864	1.446	1.463	1.34	1.372
	Relative error	0.67%	0.47%	0.42%	2.47%	0.74%	2.00%

**Figure 11.** Frequency domain diagrams of the single-frequency disturbance.

obtained using the iterative coefficient matrix. The principle prototype of the simulator is driven by the exciting force matrix, and the experimental values are obtained at last.

#### 4.2. Experimental testing

In order to test the performance of the simulator, we built a test system to test the ability of the micro-vibration simulator to simulate space six-dimensional micro-vibration. The planning scheme for the disturbance force and moment to be generated by the six-dimensional disturbance force and moment simulator is shown in Figure 9. The target values for the disturbance force and moment are known based on the theoretical model of the whole machine and the excitation forces generated by each uniaxial actuator can then be calculated. Six excitation forces are used to drive the simulator and an iterative control algorithm is added to the scheme. The actual disturbance forces and moments generated by the disturbance force and moment simulator are measured using the six-dimensional force

measurement platform (Xia et al., 2019) installed below the simulator platform.

The experimental setup for the six-dimensional disturbance force and moment simulator used to simulate micro-vibrations is shown in Figure 10. This setup mainly includes a computer (1), a control box ((2), with a power supply, a Beckhoff controller, a Beckhoff output terminal and a linear power amplifier), the six-dimensional disturbance force and moment simulator (3), a six-dimensional force measurement platform (4), and a signal acquisition instrument (5). The function of the computer in this setup is to send instructions and receive the feedback signals. The computer inputs the written program into the Beckhoff controller, which then transmits a voltage signal to the power amplifier via its voltage output terminal. In addition, the power amplifier converts the voltage signal into a current signal to be input to the six-dimensional disturbance force and moment simulator. The simulator is connected to the six-dimensional force measurement platform, which collects the disturbance forces and moments generated at

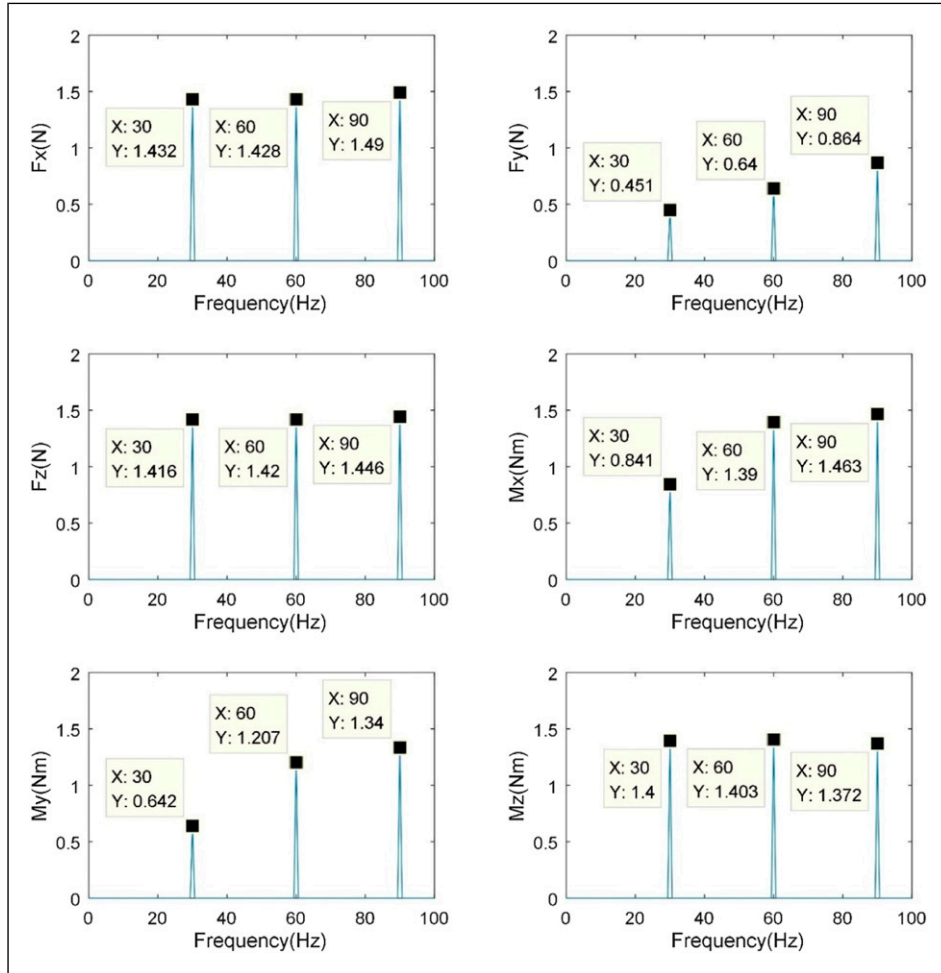


Figure 12. Frequency domain diagrams of the multi-frequency disturbance.

the center of the simulator. In addition, the computer receives the collected feedback signals to obtain the actual values of the six-dimensional disturbance forces and moments.

The first six modes of the six-dimensional disturbance force and moment simulator are at 13.415 Hz. The simulator consists of six single-degree-of-freedom actuators. The single-degree-of-freedom actuator adopts the structure of voice coil motor and spring in parallel. The first-order natural frequency is 13.415 Hz. For excitation above 15 Hz, the influence of structural resonance can be avoided. With the increase of frequency, the effect of elastic force will decrease significantly, which can be equivalent to an ideal force actuator (Keas et al., 2012). When the simulator works, it will produce structural resonance at the natural frequency. When the natural frequency exceeds a certain range, the influence of structural resonance will be attenuated. Therefore, the range of working bandwidth should avoid the natural frequency. The working bandwidth of the proposed simulator is 15 Hz–250 Hz. In the low frequency range, 20 Hz is selected as the operating frequency for the single-frequency experiment. Using the data given in Table 2, the six-dimensional disturbance force and moment simulator was tested by performing the single-frequency experiment. The disturbance force was obtained for each actuator using equation (11) and the disturbance forces and moments were simulated by controlling the driving force for each actuator. The frequency domain diagram of the experimental results for the single-frequency disturbance is shown in Figure 11. The values for each frequency point in Figure 11 are compared with the data given in Table 2 and the relative errors between the values are then calculated. The maximum error recorded in the single-frequency experiment for the disturbance force and moment simulator was 1.90%.

A multi-frequency experiment was then performed on the six-dimensional disturbance force and moment simulator. The disturbance forces and moments in Table 3 were selected as the disturbance targets for the simulator. The frequencies for each disturbing force and moment were consistent with the corresponding values for the flight reaction wheel (Zhou et al., 2012). The disturbance force for each actuator was obtained using equation (11) and the driving force for each actuator was controlled to simulate the required six-dimensional disturbance force and moment. The results of the multi-frequency disturbance experiment are shown in Figure 12. The values at each frequency point in Figure 12 are compared with the data shown in Table 3. Table 3 shows that the maximum error for the disturbance force and moment simulator is 2.96% and that the error is consistently less than 10%, which meets the requirements for practical engineering application.

## 5. Conclusions

Because of the lack of a suitable vibration source for use in ground-based experiments, a novel six-dimensional

disturbance force and moment simulator is designed and experimentally tested in this work. The novel simulator realizes the required six-dimensional disturbance force and moment output using the reaction force that is generated using six uniaxial actuators in an appropriate spatial distribution. The simulator is greatly simplified in terms of both its structural and the dynamic modeling required. Additionally, the proposed simulator overcomes the disadvantage of the Gough–Stewart platform with its hinge gap. Based on the equivalent principle of force system, a theoretical model of the six-dimensional disturbance force and moment simulator is established and the complete theoretical model is verified by experimental testing. The maximum error between the experimental and target force and moment values is 2.96%. The result is verified that the proposed six-dimensional disturbance force and moment simulator provides a micro-vibration environment for use in ground experiments and thus lays a foundation for the development of space-based optical loads with high resolution and high stability.

## Declaration of conflicting interests

The author(s) declared no potential conflicts of interest with respect to the research, authorship, and/or publication of this article.

## Funding

The author(s) disclosed receipt of the following financial support for the research, authorship, and/or publication of this article: This work was supported by the National Natural Science Foundation of China [grant numbers 11672290, 51705083] and the Key-Area Research and Development Program of Guangdong Province [No.2020B0404020002].

## ORCID iD

Zhenbang Xu  <https://orcid.org/0000-0002-4120-2448>

## References

- Asadi F and Sadati SH (2017) Full dynamic modeling of the general Stewart platform manipulator via kane's method. *Iranian Journal of Science and Technology: Transactions of Mechanical Engineering* 42: 161–168.
- Bianco V, Mandracchia B, Marchesano V, et al. (2017) Endowing a plain fluidic chip with micro-optics: a holographic microscope slide. *Light: Science & Applications* 6: e17055.
- Chen S, Xuan M, Xin J, et al. (2020) Design and experiment of dual micro-vibration isolation system for optical satellite fly-wheel. *International Journal of Mechanical Sciences* 179: 105592.
- Han JH, Park G and Lee DO (2014) Development of multi-degree-of-freedom microvibration emulator for efficient jitter test of spacecraft. *Journal of Intelligent Material Systems and Structures* 25(9): 1069–1081.
- Hehlen MP, Meng J, Albrecht AR, et al. (2018) First demonstration of an all-solid-state optical cryocooler. *Light: Science & Applications* 7(1): 15.

- Keas PJ, Dunham E, Lampater U, et al. (2012) Active damping of the SOFIA Telescope assembly. *Proc Spie* 8444: 11.
- Lin L, Tan L, Lin K, et al. (2018) The influence of flywheel micro vibration on space camera and vibration suppression. *Mechanical Systems and Signal Processing* 100: 360–370.
- Liu C, Jing X, Daley S, et al. (2015) Recent advances in micro-vibration isolation. *Mechanical Systems and Signal Processing* 56: 55–80.
- Liu KC, Kenney T, Maghami P, et al. (2007) Jitter test program and on-orbit mitigation strategies for solar dynamic observatory. In: 20th International Symposium on Space Flight Mechanics, Annapolis, MD, September 24, 2007.
- Luo Q, Li D, Zhou W, et al. (2013) Dynamic modelling and observation of micro-vibrations generated by a single gimbal control moment gyro. *Journal of Sound & Vibration* 332(19): 4496–4516.
- Oftadeh AT (2010) Explicit dynamics formulation of Stewart-Gough platform: a Newton-Euler approach. *IEEE/RSJ International Conference on Intelligent Robots & Systems*.
- Park G and Han JH (2012) Development of multi-dof active microvibration emulator using voice coil motor. *ASME Conference on Smart Materials*.
- Qin C, Xu Z, Xia M, et al. (2020) Design and optimization of the micro-vibration isolation system for large space telescope. *Journal of Sound and Vibration* 482: 115461.
- Sun YH, Zhang YW, Hu D, et al. (2018) Nonlinear energy sink for a flywheel system vibration reduction. *Journal of Sound and Vibration* 429: 305–324.
- Wang B (2017) Optimization and design of a parallel platform combined vibration-isolation with pointing. *Changchun Institute of Optics, Precision Machinery and Physics, Chinese Academy of Sciences*.
- Wang X, Xu Z, Xia M, et al. (2018) Research on a six-degree-of-freedom disturbance force and moment simulator for space micro-vibration experiments. *Journal of Sound & Vibration* 432: 530–548.
- Wu Y, Yu K, Jiao J, et al. (2015) Dynamic modeling and robust nonlinear control of a six-DOF active micro-vibration isolation manipulator with parameter uncertainties. *Mechanism & Machine Theory* 92: 407–435.
- Xia M, Xu Z, Han K, et al. (2019) Dynamic disturbance force measurement platform for large moving device in spacecraft. *Journal of Sound and Vibration* 447: 61–77.
- Xu Z, Zhu D, He S, et al. (2019a) Optimization of spatial micro-vibration simulation platform. *Optics and Precision Engineering* 27(12): 2590–2601.
- Xu ZD, Huang XH, Xu FH, et al. (2019b) Parameters optimization of vibration isolation and mitigation system for precision platforms using non-dominated sorting genetic algorithm. *Mechanical Systems and Signal Processing* 128: 191–201.
- Yang J, Xu Z, Wu Q, et al. (2016) Dynamic modeling and control of a 6-DOF micro-vibration simulator. *Mechanism & Machine Theory* 104: 350–369.
- Zhang J, Guo Z and Zhang Y (2016) Dynamic characteristics of vibration isolation platforms considering the joints of the struts. *Acta Astronautica* 126: 120–137.
- Zhou W, Dongxu LI, Luo Q, et al. (2012) Analysis and testing of microvibrations produced by momentum wheel assemblies. *Chinese Journal of Aeronautics* 25: 640–649.
- Zhou WY, Aglietti GS and Zhe Z (2011) Modelling and testing of a soft suspension design for a reaction/momentum wheel assembly. *Journal of Sound and Vibration* 330(18–19): 4596–4610.